01 Dec 2020

Innovative Approach to Repair Corroded Steel Piles using Ultra-High Performance Concrete

Binod Shrestha

Ahmed Gheni

Mohanad M. Abdulazeez

Mohamed ElGawady
Missouri University of Science and Technology, elgawadym@mst.edu

Recommended Citation

B. Shrestha et al., "Innovative Approach to Repair Corroded Steel Piles using Ultra-High Performance Concrete," *Transportation Research Record: Journal of the Transportation Research Board*, vol. 2674, no. 12, pp. 1-14, SAGE Publications, Dec 2020.
The definitive version is available at https://doi.org/10.1177/0361198120929329

TRR
JOURNAL OF THE TRANSPORTATION RESEARCH BOARD

Research Article

Transportation Research Record
2020, Vol. 2674(12) 1–14

DOI: 10.1177/0361198120929329
journals.sagepub.com/home/trr
SAGE

Innovative Approach to Repair Corroded Steel Piles using Ultra-High Performance Concrete

Binod Shrestha[1], Ahmed Gheni[1], Mohanad M. Abdulazeez[1], and Mohamed A. ElGawady[1]

Abstract

Steel H-piles are a common structural system in existing bridges. Many steel H-piles have been corroded as a result of severe weather and acid/alkaline salt exposures, causing a reduction in the axial load capacity. This paper experimentally investigates the use of ultra-high performance concrete (UHPC) encasement as a novel repair method for corroded steel H-pile. UHPC displays better tensile strength, early compressive strength, workability, and durability compared with conventional concrete. The proposed repair is used to bridge the corroded section in H-pile using either a cast-in-place or precast UHPC elements. A series of push-out tests was conducted on eight full-scale piles to assess the axial force that can be transferred through shear studs and bond between the UHPC and steel piles. The test parameters include the type of casting of the UHPC, that is, cast-in-place versus precast elements, thickness and shape of the UHPC elements, an inclusion of carbon fiber reinforced polymer (CFRP) grid, number and grade of bolts, an inclusion of washer, and applying torque on the bolts. The experimental work demonstrated that the UHPC precast repair can be easily implemented. Moreover, using 57 mm (2.25 in.) thick UHPC plates reinforced by two layers of the CFRP grid was capable of transferring up to 81% of the squash load of the H-pile.

Steel H-piles are commonly used as a substructure in bridge construction in the U.S. Some of these piles are subjected to acidic environmental exposure, repeated wet–dry cycles, or both, causing corrosion which leads to section loss and reduction in their axial load capacities, compromising the integrity of the bridges supported by these piles (*1–3*). Therefore, these corroded steel H-piles are in urgent need of repair.

Various methods such as concrete encasement (*4*), fiber-reinforced polymer (FRP) wrapped concrete encasement (*5–7*), and addition of welded or bolted steel plate (*8*) were used, by many departments of transportation in the U.S., to repair H-piles. However, these repair methods are challenging to implement and add heavyweight to the existing piles (*9, 10*).

An emerging candidate for the repair of infrastructure is ultra-high performance concrete (UHPC). UHPC has improved tensile strength, early compressive strength, workability, and durability compared with conventional concrete (*11–14*). Recently, UHPC has received considerable attention in new construction and repair of infrastructure (*15–17*). Using UHPC member can reduce the required concrete section depth compared with that of conventional reinforced or prestressed concrete sections, which reduces the weight of UHPC sections compared with its counterpart sections by up to 70% (*18*).

Farzad et al. investigated the performance of UHPC as a repair material to replace the damaged normal strength concrete in reinforced concrete bridge columns subjected to a combination of static axial and cyclic lateral loads (*16*). The experimental results revealed that such replacement increased the lateral strength of the repaired columns without increasing their sizes.

Zmetra et al. have studied the effectiveness of cast-in-place UHPC encasing corroded region of W-shaped simply-supported steel girders having shear studs welded to the web and bottom flange (*19*). The UHPC had a thickness ranging from 44.5 mm (1.75 in.) to 50 mm (2 in.), which was selected to provide sufficient cover to the studs installed on the flange and web. The load-carrying capacity of the UHPC-repaired girder increased by 430% compared with that of the damaged

[1]Department of Civil, Architectural and Environmental Engineering, Missouri University of Science and Technology, Rolla, MO

Corresponding Author:
Mohamed A. ElGawady, elgawadym@mst.edu

girder. Similarly, Kruszewski and Zaghi studied a UHPC encasement of a corroded W-shaped steel beam using three different types of shear connectors: headed studs, threaded bars, and UHPC dowels attached to the web of the beam (*20*). The repair method with the headed studs and with the threaded bars showed a ductile mode of failure, whereas with UHPC dowel exhibited a brittle failure mechanism. Overall, the UHPC repair encasement reduced the strains accumulation on the damaged portion of the web and thereby increased the strength of the repaired specimens compared with that of the reference specimen without any damage to the web plate.

The behavior of a composite section consisting of H-shaped steel section having shear connectors installed in its flanges and encased in UHPC was investigated through the push-out testing (*21*). The UHPC had high splitting tensile strength and therefore improved the interfacial shear strength and stiffness.

The use of FRP as internal reinforcement in UHPC was investigated (*22–24*). Adding carbon fiber-reinforced polymer (CFRP) as internal reinforcement increased the UHPC tensile strength and so improved the performance of the UHPC elements. Michael et al. showed a significant improvement in ductility for concrete cylinders with an embedded CFRP grid compared with the cylinders without the CFRP grid (*25*). Using a CFRP grid embedded in UHPC panels enhanced its flexural performance and ductility (*26*).

The applications of UHPC as a repair material for structural elements, including beam-column joints, reinforced concrete columns and slabs, and steel bridge girders displayed a good structural response. However, there have been no studies investigating the feasibility of using UHPC to repair corroded steel columns. This paper uses push-out tests to evaluate the interfacial shear between the UHPC and the steel piles. Both cast-in-place (CIP) and prefabricated (PF) UHPC encasement are proposed as a repair method to increase the load-carrying capacity of corroded steel H-piles. The UHPC was either unreinforced or reinforced using CFRP grids. Shear connectors (SCs) were used to connect the UHPC to the steel piles.

Research Significance

This paper presents the experimental results of the push-out test conducted on eight full-scale steel H-piles encased in UHPC. The main objective of this manuscript is to develop UHPC repair solution that can bridge a corroded section, L_{cor} in Figure 1, in an H-pile. During the push-out test, a gap of 50 mm (2 in.) was used underneath each steel pile (Figure 2). Such gap represented 100% losses in a pile cross-section caused by corrosion, that is, L_{cor} is simulated as a gap. Therefore, the push-out tests were used to assess the axial force that can be

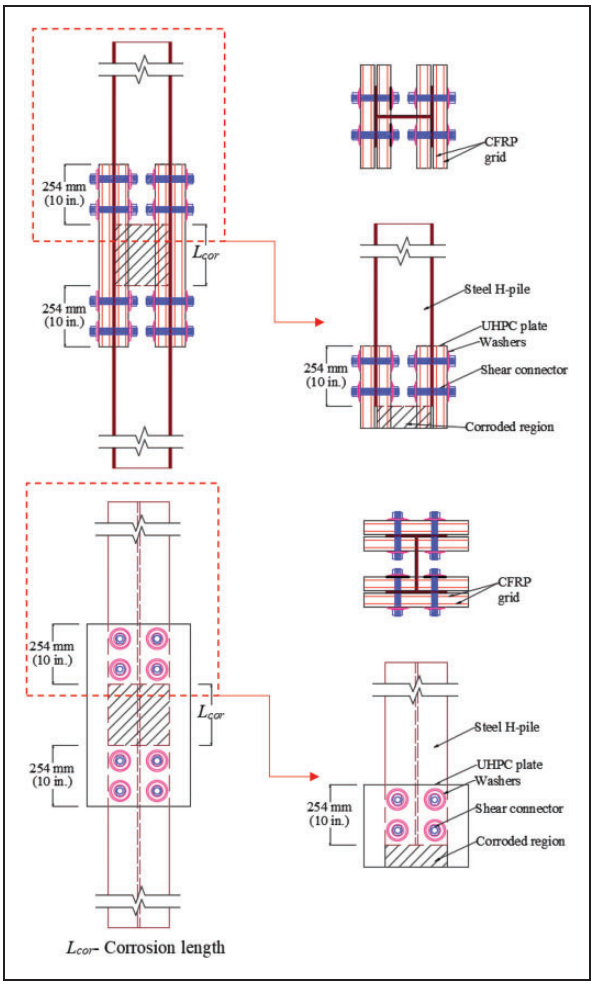

Figure 1. Ultra-high performance concrete (UHPC) encasement for the repair of the steel H-pile.
Note: CFRP = carbon fiber-reinforced polymer.

transferred through shear studs and bond between the UHPC and steel piles.

The development of the UHPC CIP sections and PF panels used in this experimental work was based on different construction factors. Considering manual-lifting related injuries, the National Institute of Occupational Safety and Health also recommends the maximum weight an industrial worker could lift, under ideal conditions, is to be about 51 pounds (*27*). The UHPC plates need to be as small as possible such that they can be handled in a construction site with minimal need for large mechanical equipment. Therefore, the thickness of the PF UHPC plates ranged from 38 mm to 76 mm (1.5 in. to 3 in.), which yielded a weight of the plates ranging from 7.25 kg to 18.18 kg (16 lbs to 40 lbs) per foot long of the proposed plates. It is worth noting that the maximum weight that an industrial worker can lift, under ideal conditions and considering manual-lifting related injuries, is about 23.13 kg (51 lbs) (*27*). Furthermore, UHPC is a

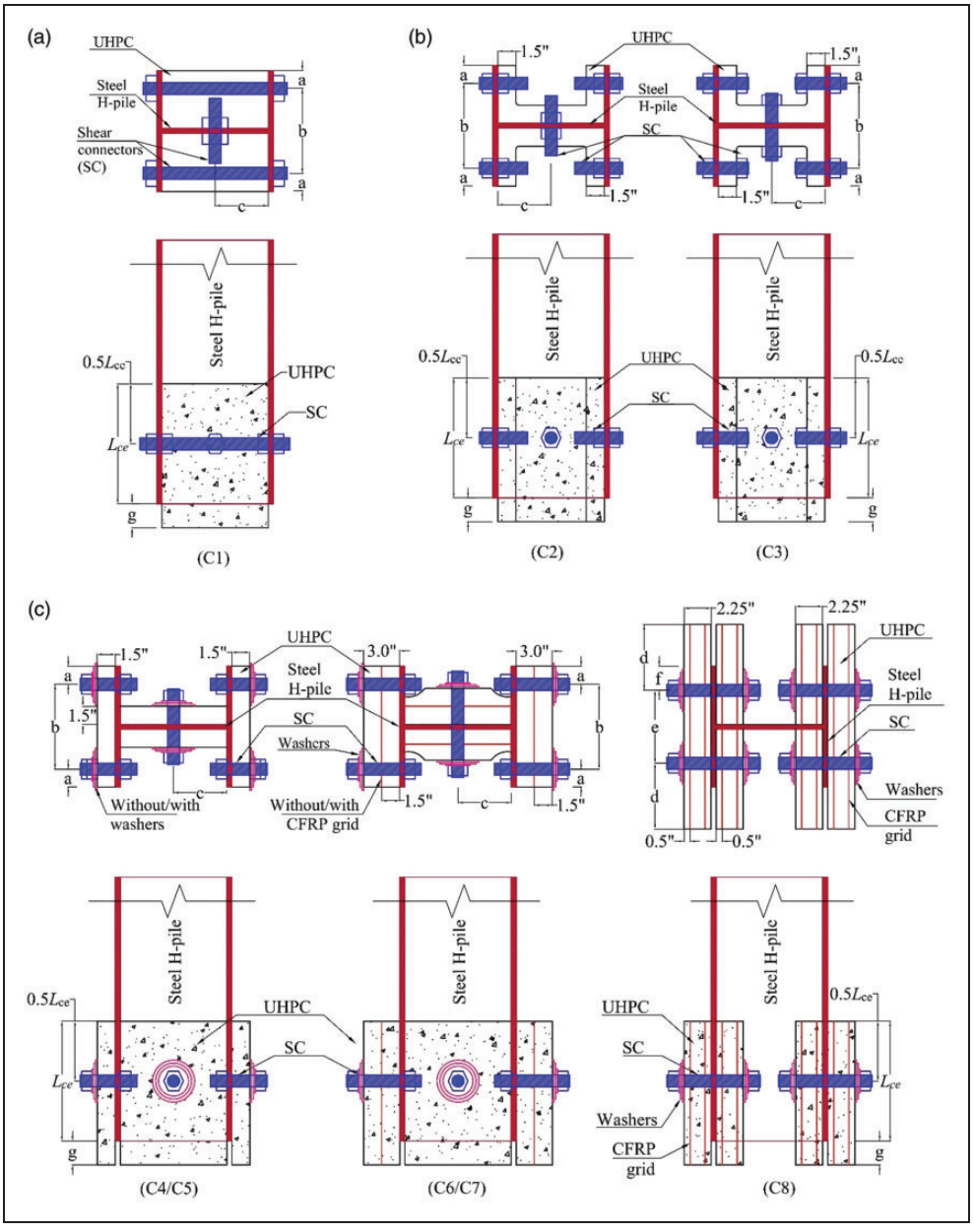

Figure 2. Test specimens. (*a*) UHPC prism, (*b*) UHPC C-shaped, and (*c*) UHPC plate. a = 38.1 mm (1.5 in.), b = 178 mm (7 in.), c = 112.5 mm (4.43 in.), d = 140 mm (5.5 in.), e = 152.4 mm (6 in.), f = 50.8 mm (2 in.), L_{CE} = 254 mm (10 in.), g = 50.8 mm (2 in.).
Note: CFRP = carbon fiber-reinforced polymer; SC = shear connector; UHPC = ultra-high performance concrete.

quite expensive material, and keeping its volume at minimal reduces the repair cost. It was recommended also to keep the thickness of a cementitious composite laminate plate in the range of 50–100 mm (2–4 in.) (*28–30*). Furthermore, although the UHPC material is generally more expensive than conventional concrete, using PF UHPC will certainly accelerate the repair by cutting the repair time from days to hours, which would compensate for the increase in UHPC material cost, ending with a cheaper repair method.

Experimental Program

Test Program

Eight full-scale 250 mm × 62 kg/m (10 in × 42 lb/ft) steel H-piles were subjected to push-out testing to investigate the shear transfer between UHPC sections having different shapes and the H-piles. The UHPC was CIP in the cases of C1 and C2 specimens and PF in the cases of C3 through C8 (Table 1). The CIP UHPC was in the form of

Table 1. Test Program

Specimen	UHPC Shape	UHPC Cast	UHPC Thickness (t_{UHPC}) mm (in.)	Shear connector Type	Shear connector Tensile strength, MPa (ksi)	Shear connector No. Flanges	Shear connector No. Web	Washer	CFRP grid layer, No.
C1	Prism	CIP	na	Threaded rod	413 (60)	2	2	No	0
C2	C	CIP	38 (1.50)	Threaded rod	413 (60)	4	2	No	0
C3	C	PF	38 (1.50)	HS bolt	1,034 (150)	4	2	No	0
C4	Plate	PF	38 (1.50)	HS bolt	1,034 (150)	4	2	No	0
C5	Plate	PF	38 (1.50)	HS bolt	1,034 (150)	4	2	Yes	0
C6	Plate	PF	76 (3.00)	HS bolt	1,034 (150)	4	2	Yes	0
C7	Plate	PF	76 (3.00)	HS bolt	1,034 (150)	4	2	Yes	1
C8	Plate	PF	57 (2.25)	HS bolt	1,034 (150)	4	0	Yes	2

Note: CIP = cast-in-place; PF = prefabricated; HS = high strength; CFRP = carbon fiber reinforced polymer; ksi = kips per square inch; na = not applicable.

228 × 122 × 305 mm (9 × 4.8 × 12 in.) prism and C-shaped sections (Figures 2, *a* and *b,* and 3, *a* and *b*). The PF was in the form of C-shaped (Figures 2*b* and 3*c*) and 38.1 mm (1.5 in.) to 76 mm (3 in.) thick plates (Figures 2*c* and 3, *d* and *e*). All UHPC shapes had a height of 305 mm (12 in.). SCs in the form of threaded rods and high-strength (HS) bolts were used for the CIP and PF UHPC sections, respectively. The UHPC elements were reinforced using 0 to 2 layers of CFRP grid embedded in the UHPC (Table 1). Specimens with and without washers were investigated as well.

Material Properties

Steel H-Pile. The mechanical properties of the steel H-piles were determined (Table 2) by performing a tensile test on three replicate steel coupons, cut from each of the flanges and webs portion of a pile, as per ASTM E8/E8M-16a (*31*).

UHPC. UHPC was prepared using high early strength Portland cement type III, ground granulated blast furnace slag, fine dry river sand, and water (Table 3). Polycarboxylate high-range water reducer (HRWR) having a solid mass content of 23% was used to enhance the UHPC workability. Straight 0.2 mm (0.0079 in.) diameter and 13 mm (0.51 in.) long micro steel fibers were used, at a volume fraction of 2% of the UHPC volume, to enhance the mechanical properties of the UHPC. The tensile strength and elastic modulus of the steel fiber were 1.9 GPa (275.57 kips per square inch [ksi]) and 203 GPa (29,442.7 ksi), respectively.

The UHPC mixing started by mixing the fine sand and steel fibers into an Eirich mixer for 2 min; that was followed by gradually adding and mixing about 50% of the total water for another 2 min. After that, the cementitious materials were added and mixed for 3 min. Then, the remaining water, mixed with HRWR, was added and the mixing was continued for another 8 min.

SCs and Washers. Two types of 25.4 mm (1 in.) diameter SC were used to connect the UHPC elements to the steel piles. The threaded rods SC with grade ASTM A307 (*32*) with a minimum tensile strength of 413.69 MPa (60 ksi) were used for the CIP UHPC elements, whereas HS SC of grade ASTM A490 (*33*) with a minimum tensile strength of 1,034 MPa (150 ksi) were attached to the steel H-pile using heavy-hex nuts and were used for the PF UHPC elements. Furthermore, washers with outer diameter/thickness of 51 mm (2 in.)/3.4 mm (0.134 in.), 76 mm (3.0 in.)/4 mm (0.156 in.), and 89 mm (3.5 in.)/3.6 mm (0.140 in.) were used in specimens C5 through C8, between the UHPC and heavy-hex nuts to disperse stress caused by the bolts (Figure 2*c*).

CFRP Grid. CFRP grids (Table 4) were embedded in the UHPC plates in the specimens C7 and C8 (Figures 2*c* and 3*d*). The nominal spacing of the CFRP grid is 41 mm (1.6 in.) × 46 mm (1.8 in.) as supplied by the manufacturer TechFab® (Figure 3*d*).

Preparation of the Test Specimens

The preparation of the test specimens was varied from the specimens, including CIP UHPC, that is, C1 and C2 to those including PF UHPC, that is, C3 through C8. The steel H-piles of specimens C1 and C2 were cleaned using a power hand tool to remove dirt, dust, rust, and mill scale per the Society for Protective Coatings Standards (*34*). The required number of threaded rods was passed through holes that had been drilled in the web and flanges of the steel H-piles. The threaded rods were attached to the piles using heavy-hex nuts (Figure 3, *a* and *b*). The H-piles were then placed atop of a 50.8 mm (2 in.) high H-shaped foam section. A pair of wooden plates, for C1, or

Table 2. Mechanical Properties of Steel H-Pile

Section	Yield stress*, MPa (ksi)	Ultimate stress*, MPa (ksi)	Elastic modulus*, GPa (ksi)	Rupture strain, mm/mm (in./in.)
Web	407 (59)	503 (73)	182 (26,400)	0.087
Flange	324 (47)	517 (75)	181 (26,250)	0.098

*Average value of three replicate specimens

Table 3. Mixture Design of the UHPC

w/c*	Cement type III kg/m^3 (lb/yd^3)	Slag kg/m^3 (lb/yd^3)	Fine sand kg/m^3 (lb/yd^3)	HRWR kg/m^3 (lb/yd^3)	Water kg/m^3 (lb/yd^3)	Steel fiber kg/m^3 (lb/yd^3)
0.2	945 (1,593)	220 (371)	1,008 (1,699)	43.8 (73.8)	200 (337)	157 (265)

Note: UHPC = ultra-high performance concrete; HRWR = high range water reducer; lb/yd3 = pound per cubic yard.
*Ratio of the total liquid (water content in HRWR and water) to the cementitious materials (cement and slag).

Table 4. Mechanical Properties of an Individual Strand of CFRP Grid per Manufacturer's Data

Direction	Tensile strength per unit width, kN/m (lb/ft)	Tensile modulus of elasticity, GPa (ksi)	Elongation at break, %
Transverse	79.9 (5,480)	234.5 (34,000)	0.76
Longitudinal	80.75 (5,530)	234.5 (34,000)	0.76

Note: CFRP = carbon fiber reinforced polymer; lb/ft = pound per foot.

plastic panels, for C2, was fixed to the sides of the webs using clamps to create the required UHPC prism or C-shaped, respectively (Figure 3, *a* and *b*).

For specimens using the PF UHPC, the C-shaped formworks (Figure 3*c*) and the wooden formworks were prepared (Figure 3*d*). The CFRP grids were cut to the required dimensions and the ends were embedded on the sides of the formwork. Concrete covers of 38.1 mm (1.5 in.) and 12.7 mm (0.5 in.) were provided for single layer of the CFRP grid in the case of C7 and for double layers in the case of C8, respectively (Figure 2*c*).

UHPC Casting and Curing of Test Specimens. The UHPC displayed a mini-slump flow spread test, per ASTM C1437 (*35*), ranging from 254 mm (10 in.) to 304 mm (12 in.). The UHPC was placed (Figure 3) in the test specimens without using any means of vibrators or tamping rod. Several 50.8 mm (2 in.) standard cubes and 76.2×152.4 mm (3×6 in.) cylinders were cast. After casting, the specimens were covered with plastic sheets to prevent moisture loss and were demolded after 24 h of placing the UHPC. The CIP specimens were covered with wet burlap sheets and cured at ambient temperature until the day of testing, whereas the PF specimens were cured in a steam chamber at a temperature of 70°C (158°F) for 24 h. The steam-cured specimens were then stored in a moisture room with a relative humidity of $95 \pm 5\%$ until the day of testing. The cubes and cylinders were exposed to curing regimes similar to those of the corresponding CIP and PF specimens. The casting and curing processes were carried out based on ASTM C1856/C1856M (*36*).

Specimen Fabrication. After gaining a target compressive strength as mentioned in Table 5, the curing was stopped. The H-shaped foam was removed from underneath the CIP specimens and the gap was cleaned from any concrete debris, allowing the H-pile to slip down during the push-out test. The PF specimens were attached to the steel H-pile with the HS bolts and heavy-hex nut, leaving a gap of 50.8 mm (2 in.) between the UHPC plates and the steel H-pile. For the specimens C3 and C4, the bolts were installed to snug tight condition, and for the C5 through C8 they were fixed with a preset torque of 9.3 kips-ft using a torque wrench.

Approximately 6.35 mm (0.25 in.) layer of hydrostone (Figure 3*e*) was placed underneath the UHPC plates to provide full contact between the UHPC plates and the base plate during the push-out testing.

Test Instrumentation and Setup

Test Instrumentation. Thirty-four strain gauges were mounted on the web and flanges of each steel H-pile of specimens C1 through C5 before placing the UHPC to measure the axial strains induced on the steel H-pile

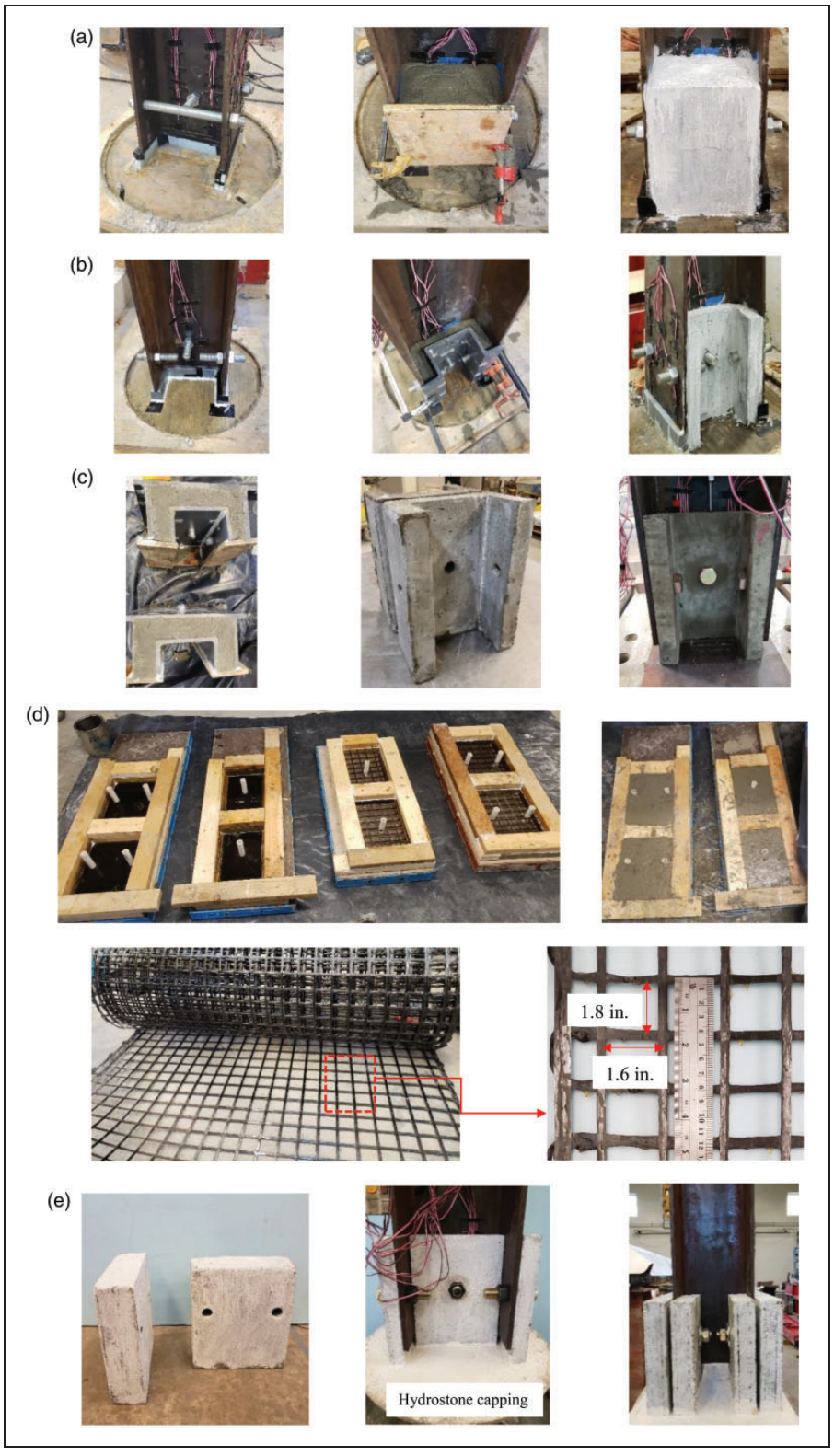

Figure 3. Test specimens preparation for (*a*) specimen C1, (*b*) specimen C2, (*c*) C-shaped UHPC, (*d*) CFRP grid and formwork for the UHPC plates, and (*e*) installation of UHPC plates.
Note: UHPC = ultra-high performance concrete; CFRP = carbon fiber reinforced polymer.

Table 5. Push-Out Test Results

Specimen	Peak load (*P*) kN (kips)	Displacement (δ_{max}*) mm (in.)	UHPC compressive strength (f'_c)** MPa (ksi)	UHPC tensile strength (f'_t)*** MPa (ksi)
C1	867 (195)	5.33 (0.21)	117.9 (17.1)	NA
C2	1,054 (237)	3.28 (0.13)	117.9 (17.1)	NA
C3	672 (151)	20.57 (0.81)	133.8 (19.4)	NA
C4	698 (157)	7.87 (0.31)	131.0 (19.0)	18.6 (2.70)
C5	787 (177)	11.00 (0.43)	131.0 (19.0)	18.6 (2.70)
C6	1,219 (274)	15.50 (0.61)	113.0 (16.4)	16.6 (2.41)
C7	1,281 (288)	39.60 (1.56)	135.8 (19.7)	18.4 (2.70)
C8	2,278 (512)	41.66 (1.64)	135.1 (19.6)	22.5 (3.26)

Note: UHPC = ultra-high performance concrete; ksi = kips per square inch; NA = not available.
*At the peak load. **For cubes on the day of the test. ***For cylinders on the day of the test.

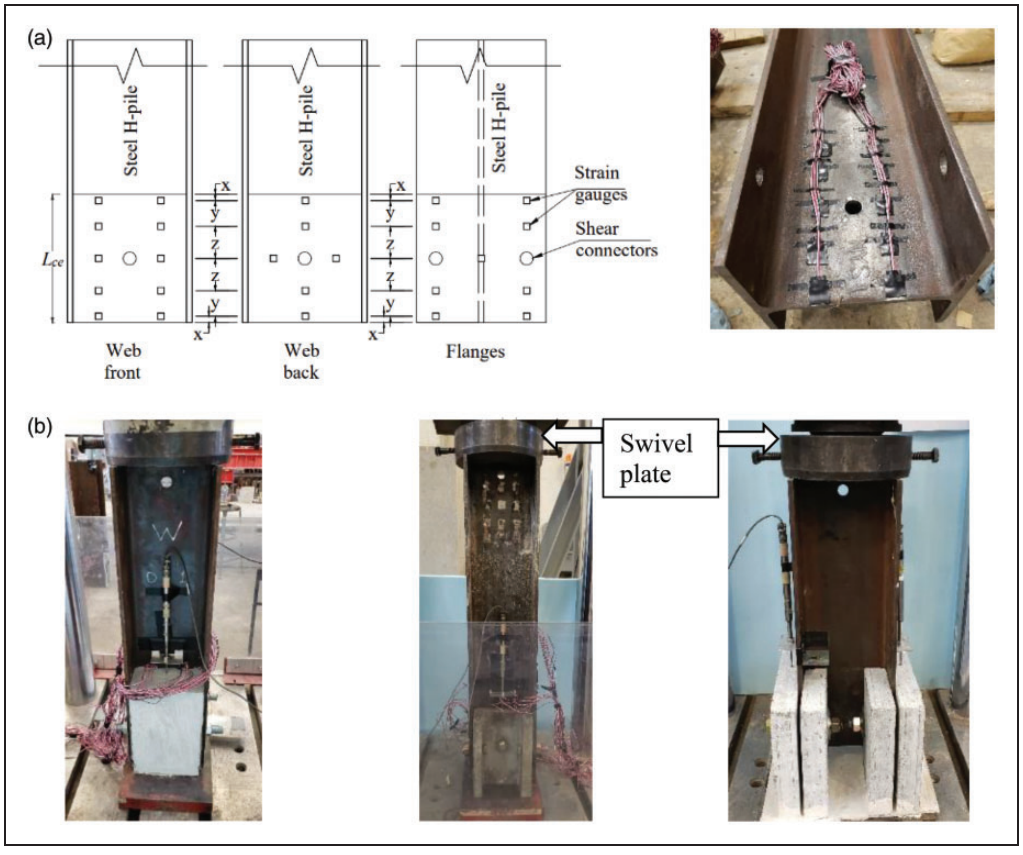

Figure 4. Test instrumentation and setup (*a*) strain gauges layout, (*b*) specimens C1, C3, and C8 (left to right) ready for testing.

during the push-out testing (Figure 4*a*). Linearly variable displacement transducers (LVDTs) were vertically located on each web, flange sides, or both, to monitor the relative axial displacement between the UHPC and the steel H-pile (Figure 4*b*).

Push-Out Testing. MTS universal testing machine with a capacity of 2,446 kN (550 kips) was used to perform the push-out testing on the steel H-piles. A MTS swivel plate was placed on the top of the steel H-pile to uniformly distribute the load from the actuator to the specimen and the bottom UHPC surface was supported on a rigid steel base forming a top-pin and bottom-hinged boundary conditions. Each specimen was aligned in the MTS testing machine to ensure the top-loading surface was horizontal. A monotonic axial load was applied, at a rate of

Figure 5. Failure modes of the test specimens: (*a*) C1, (*b*) C2, (*c*) C3, (*d*) C4, (e) C5, (*f*) C6, (*g*) C7, and (*h*) C8.

1.27 mm/min (0.05 in./min), to the top of each test specimen using the MTS swivel plate (Figure 4*b*). Data acquisition and recording were carried out at 2 Hz with a multichannel acquisition device. All the specimens were loaded until failure occurred.

Results and Discussion

The push-out test results, along with the average compressive and tensile splitting strengths of the UHPC, on the day of testing the piles, are summarized in Table 5.

Performance of the Test Specimens and Failure Modes

Figure 5 shows the specimens after testing. Figure 6 displays the axial force measured using the load cell of the MTS testing machine and the displacements measured using the LVDTs attached to each steel pile. The failure modes of the tested specimens can be categorized as: (i) shear-off of the shear connector, (ii) splitting failure of the UHPC, and (iii) breakout of the UHPC.

Both specimens C1 and C2 displayed similar force versus displacement as both were CIP specimens

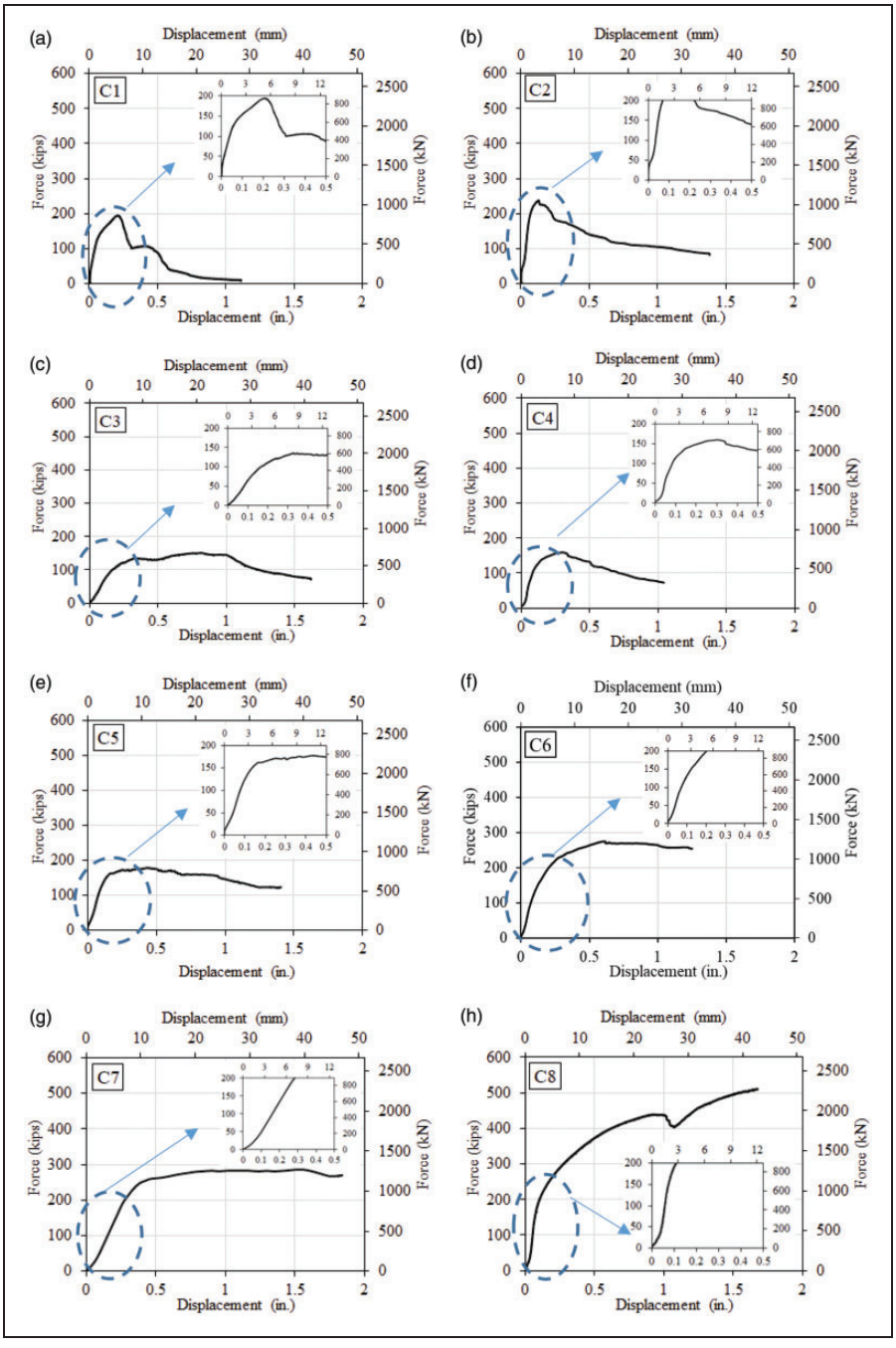

Figure 6. Axial force versus displacement for specimens: (*a*) C1, (*b*) C2, (*c*) C3, (*d*) C4, (e) C5, (*f*) C6, (*g*) C7, and (*h*) C8.

(Figure 6, *a* and *b*). Both specimens displayed a negligible slip between the steel H-pile and the UHPC, as a result of the interface bond adhesion between the pile and the UHPC, up to approximately 10% and 12% of the peak axial loads corresponding to average interfacial shear stresses of 0.43 MPa (62 pounds per square inch [psi]) and 0.56 MPa (81 psi), for specimens C1 and C2, respectively. It is worth noting that Abdulazeez et al. measured bond stress values ranging from 0.54 MPa (78 psi) to 0.84 MPa (122 psi) for conventional concrete having compressive strengths ranging from 20.6 MPa (2,990 psi) to 65.5 MPa (9,490 psi) encasing steel piles with the embedment length of 254 mm (10 in.) (*4*). Beyond debonding of the UHPC from the steel pile, slip occurred and the UHPC bore against the threaded rods and both specimens displayed different damage patterns because of the differences in the thickness of the used UHPC elements.

For the specimen C1, with the subsequent increase in the axial load up to about 556 kN (125 kips), a yielding of the threaded rods occurred without any visible UHPC cracks. With continuous loading, the specimen reached its peak load of 867 kN (195 kips) at a displacement of 5.33 mm (0.21 in.), corresponding to about 30% of the squash load of the H-pile. This was followed by a sudden drop in the axial load resulting from the shearing-off of the threaded rods attached to the flanges and web sections (Figures 5*a* and 6*a*). Failure of the rods was accompanied by a loud noise. No damage was observed in the UHPC prism at all. Using Equation 1 (*37*), the nominal shearing-off strength of the threaded rod (V_{sa}) was calculated as 1,089 kN (245 kips) which represented 125% of the experimental peak load.

$$V_{sa} = A_{se} f_{uta} \tag{1}$$

$$A_{se} = \frac{\pi}{4}\left(d_{sa} - \frac{0.969}{n_t}\right)^2 \tag{2}$$

where A_{se} = effective cross-sectional area of SC (in^2), f_{uta} = specified tensile strength of the SC (ksi), d_{sa} = diameter of the SC (in.) and n_t = number of threads per inch.

For the specimen C1 and C2, the values used for n_t, d_{sa} and f_{uta} were 14 per inch, 25.4 mm (1 in.) and 413 Mpa (60 ksi), respectively.

For the specimen C2, the first crack appeared at the level of the threaded rods attached to the flange and it was a horizontal crack extending through the thickness of the flanges of the UHPC C-shaped panel. The crack appeared at an axial load of 876 kN (197 kips), corresponding to about 31% of the squash load of the H-pile. At approximately 85% of the peak axial load, splitting diagonal cracks in the flanges of the UHPC were observed resulting from the small threaded rod edge distance, which was a = 38.1 mm (1.5 in.) (Figure 2*b*). This was followed by gradual tilting of the rods attached to the flange, leading to the steel H-pile flange outward bending at the level of the threaded rod creating a gap of approximately 12.2 mm (0.5 in.) between the steel flange and the flange of the UHPC (Figure 5*b*). The outward bending was caused by the eccentric loading because of the presence of the UHPC panel only on one side of each flange. Breakout failure of the web of the UHPC was observed at a load of 987 kN (222 kips), corresponding to 35% of the squash load of the H-pile. The specimen C2 reached a peak axial load of 1,054 kN (237 kips), corresponding to 38% of the squash load of the steel H-pile, at a displacement of 3.28 mm (0.13 in.). At the peak load, failure occurred as a result of the shearing-off of the threaded rod attached to the web section only. The existence of the rods in the flanges, however, allowed the axial load to gradually decrease compared with the case of the specimen C1 (Figure 6*b*). The threaded rods' nominal shear strength of 1,089 kN (244.8 kips), which was predicted from Equation 1, represented 103% of the experimental peak load.

Specimens C3 through C8 included PF UHPC panels and plates. The first crack in specimen C3 was a horizontal crack appearing at the level of the HS bolt in the flanges of the UHPC at the load of 418 kN (94 kips), corresponding to 15% of the pile squash load. This was followed by tilting of the bolts attached to the flanges and diagonal cracks developed above and below the bolts toward the free edge at about 80% of the peak load, splitting the UHPC at the flange side as in Figure 5*c*. With the increase in the axial load to about 605 kN (136 kips), corresponding to 22% of the pile squash load, breakout at the web of the UHPC was observed. The specimen C3 reached a peak axial load of 672 kN (151 kips), corresponding to 24% of the squash axial load of the steel H-pile, at a displacement of 20.57 mm (0.81 in.) (Figure 6*c*). Unlike specimen C2, bolts shear failure did not occur in C3 as a result of using high-strength bolts in the case of C3. Equation 3 (*37*) developed for post-installed anchors, predicted 1,455 kN (327 kips) as the stud shear strength for specimen C3, which represented 217% of the experimental peak load. Furthermore, no outward deformation of the flange of the steel H-pile occurred as in the case of C2.

$$V_{sa} = 0.6\, A_{se} f_{uta} \tag{3}$$

The first crack in each of the specimens C4 through C7 was a horizontal crack that developed at the levels of the HS bolts along the edges of the UHPC plates attached to the flanges of the steel H-pile, which is attributed to the small edge distance, equals to 38.1 mm (1.5 in.), of the bolts in the UHPC plates (Figure 2*c*).

For specimen C4, without washers, the first crack initiated at an axial load of 587 kN (132 kips), whereas for C5, with washers, it occurred at 614 kN (138 kips), corresponding to 21% and 22% of the H-pile's squash load, respectively. For the specimen C4, as the axial load increased to about 89% of peak load, UHPC breakout was observed at the flange side of the H-pile, and gradual tilting of the bolts occurred, along with inward bending of the flange of the steel H-pile. Furthermore, with an increase in the load to about 676 kN (152 kips), the UHPC plates at the web of the steel H-pile developed breakout cracks (Figure 5*d*). The specimen C4 reached a peak load of 698 kN (157 kips), at a displacement of 7.87 mm (0.31 in.), corresponding to 25% of the pile's

squash load. The specimen C5 displayed a failure mechanism similar to that of the specimen C4, that is, developing cracks in the UHPC plates attached to the flanges of the H-pile followed by cracks in those attached to the web sides of the steel H-pile (Figure 5*e*). The peak axial load for C5 was 787 kN (177 kips), corresponding to 28% of the pile's squash load, at a displacement of 11 mm (0.43 in.)

For the specimen C6, without CFRP grid, the first crack appeared at an axial load of 662 kN (149 kips), whereas for C7, with single-layer of CFRP grid, it appeared at 898 kN (202 kips), corresponding to 24% and 32% of the H-pile's squash load, respectively. With the increase in the load to about 65% and 70% of each peak load in C6 and C7, respectively, the UHPC on the flange sides developed splitting vertical cracks leading to tilting of the bolts and inward bending of the flange of steel H-pile. The peak axial loads for specimens C6 and C7 were 1,219 kN (274 kips) and 1,282 kN (288 kips), corresponding to 43% and 46% of the pile's squash load, at a displacement of 15.5 mm (0.61 in.) and 39.6 mm (1.56 in.), respectively. In both specimens, no cracks were observed on the UHPC attached to the webs of the steel H-pile (Figure 5, *f* and *g*) which led to a relatively quite ductile failure (Figure 6, *f* and *g*).

The first crack in the specimen C8, with double layers of CFRP grid, was observed at an axial load of 1,948 kN (438 kips), corresponding to about 70% of the H-pile squash load. The crack occurred in all UHPC plates as a result of UHPC breakout caused by the bearing of the bolts against the plates, along with bending of the bolts. No splitting cracks have occurred, because of sufficient edge distance from the center of the bolt holes to the edge of the UHPC plate. The specimen reached a peak axial load of 2,278 kN (512 kips), corresponding to 81% of the squash load of the steel H-pile, at a displacement of 41.66 mm (1.64 in.). The tilting of the bolts and bending of the flange section of the steel H-pile were prevented as the UHPC plates were attached to both inside and outside of the flanges, creating concentric loading conditions (Figure 5*h*). The specimen developed a very ductile failure mode (Figure 6*h*).

Discussion of the Test Results

Both specimens C1 and C2 were CIP specimens with one main difference. The UHPC had different shapes, that is, prism and C-shaped in the case of C1 and C2 specimens, respectively. The change in the shape resulted in different embedded lengths of 114 mm (4.5 in.) and 38.1 mm (1.5 in.) for the bolts in C1 and C2, respectively. Changing the embedded length of bolts changed the mode of failure from bolts shear-off failure in the case of the specimen C1 to UHPC breakout crack in the flange side, followed by shear-off of the bolts attached to the web in the case of the specimen C2, which increased the ultimate load by 21.5% only.

The specimen C3 was similar to the specimen C2, but the C3 incorporated PF UHPC whereas the C2 incorporated CIP UHPC. Furthermore, the specimen C2 used A307 threaded rods whereas the specimen C3 used A490 HS bolts. However, the specimen C3 displayed 36% lower strength than that of the C2 (Figure 6*c*) because of the uniform distribution and transfer of the interface bond shear stresses between the UHPC and steel pile in the case of C2 compared with the stress concentration at the bolt location in the case of C3.

Specimens C4 and C5 were identical except that washers were used in the specimen C5. Adding washers in the case of the specimen C5 decreased the bolt stress and increased the friction between the steel H-pile and the UHPC (Figure 6, *d* and *e*), leading to 13% higher strength in the case of the specimen C5. Furthermore, the post-peak decrease in strength in the case of the specimen C5 was gradual compared with that of the specimen C4.

Specimens C5 and C6 were identical except for the thickness of the UHPC plates. Increasing the thickness of the UHPC plate by 100% from 38 mm (1.5 in.) in the case of C5 to 76 mm (3 in.) in the case of C6, the axial load increased by 55% from 787 kN (177 kips) to 1,219 kN (274 kips) (Figure 6, *e* and *f*). This occurred as a result of increasing the splitting and breakout strength of the UHPC with increasing the thickness of the UHPC plate. Furthermore, doubling the thickness of the UHPC did not change the mode of failure.

Specimens C6 and C7 were identical except that C7 incorporated one layer of the CFRP grid. Adding CFRP grid significantly reduced the number of cracks in the UHPC plates and delayed the initiation of the first crack. The first crack in the case of the specimen C7 occurred at an axial load of 898 kN (202 kips), which is approximately 35% higher than that of the specimen C6. However, adding the CFRP grid increased the load-carrying capacity by 5% only (Figure 6, *f* and *g*).

The highest axial load capacity was observed in the case of specimen C8, with two layers of CFRP grid embedded in the UHPC plates, bolted only to the flange section of the steel H-pile. The specimen C8 was able to reach an axial capacity of 2,278 kN (512 kips), representing an improvement of 78% compared with the specimen C7 (Figure 6*h*). The improvement in the axial load occurred because of doubling the number of CFRP grid and increasing the number of bolts by 33% compared with that of the specimen C7. Furthermore, the bolts in the specimen C8 were double-shear, whereas all the bolts in the other specimens were single-shear. In the specimen C8, the UHPC edge distance from center of the bolt is significantly higher (about 3.5 times) than that

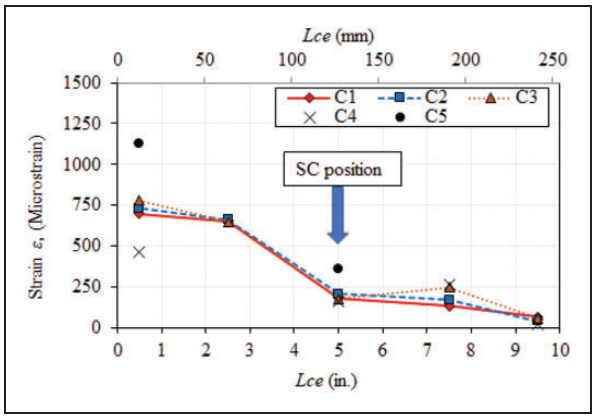

Figure 7. Axial strain distribution along with the embedded depth at the peak load.
Note: SC = shear connector; Lce = embedment length.

of the other specimens. Using larger edge distance eliminated the splitting failure that occurred in the other specimens.

Bond Strain Distribution

The axial strain distribution of each steel H-pile for the first five specimens from C1 to C5 along a depth of 254 mm (10 in.) are shown in Figure 7. The strains were measured using the average readings of the strain gauges attached to the flanges and web of a section of the steel H-piles. In Figure 7 the zero value and 254 mm (10 in.) reading along L_{ce} represent the loaded end and free end of the steel H-pile respectively. In general, the axial strain distribution indicated higher strain values close to the loaded end and decreased along the embedded length toward the free end. The strain gauges located at L_{ce} of 63.5 mm (2.5 in.) for specimens C4 and C5 were malfunction and therefore their readings at this section are not presented in Figure 7. Compared to the strains at the loaded end, the average axial strain at the location of the shear connectors was 29% of that measured at the loaded end. This indicates that in all specimens, including the CIP C1 and C2, the load is mainly transferred from the steel H-pile to the UHPC using the shear connectors.

Conclusions

Steel H-piles are common structural system in many bridges across the U.S. Some of these steel H-piles have been corroded through exposure to severe weather and acid/alkaline salts, causing reductions in the axial load capacities of these piles, leading to compromising the integrity of the bridges supported by these piles. This paper experimentally investigates the use of UHPC encasement as a novel repair method for corroded steel H-pile. CIP UHPC and PF UHPC plates were proposed to bridge the corroded section in a H-pile. The PF UHPC plates represent a lightweight rapid repair solution. The behavior of the repaired piles was investigated using a monotonic push-out static testing. The effects of washers, plate thickness, and the inclusion of CFRP grid reinforcement in UHPC on the axial load strength were investigated. The following conclusions were drawn from the experimental testing:

1. The average interfacial shear stresses between the CIP UHPC and steel piles ranged from 0.43 MPa (62 psi) to 0.56 MPa (81 psi). This is quite similar to values measured earlier for conventional concrete.
2. For the CIP UHPC, changing the stud embedment length-to-diameter from 4.5 in C1 to 1.5 in C2 changed the mode of failure. In the case of C1, shearing-off of the threaded rods was observed with no damage at all to the UHPC. For the C2, a combination of shear-off of the threaded rod and breakout of the UHPC was observed.
3. Using ACI 318 (*37*) predicted quite well the shearing-off strengths of the studs in the CIP UHPC. The predicted strengths ranged from 125% to 103% of the measured strengths.
4. Using high-strength bolts, no shear-off of the studs occur red and failure in specimens C3 through C8 occurred because of UHPC breakout.
5. Adding washers to the bolts used to install the UHPC plates decreased the bolt stresses and increased the friction between the steel H-pile and the UHPC (Figure 6, *d* and *e*), leading to 13% higher strength.
6. Increasing the thickness of the UHPC plate increased the breakout strength. However, the increase is not linear. Increasing the UHPC thickness by 100% from 38 mm (1.5 in.) to 76 mm (3 in.), the breakout strength increased by 55%.
7. Adding a CFRP grid layer significantly reduced the number of cracks and increased the cracking load by 35% but did not significantly increase the ultimate load.
8. Using well-designed PF UHPC plates was able to cover 81% of the squash load of the H-pile. Furthermore, the proposed system is easy and fast to install. The plates also are relatively lightweight and more durable than conventional concrete or steel plates. However, further research is still needed to develop design guidelines for the prefabricated plates.

Authors' Note

Ahmed Gheni is now affiliated with Department of Civil Engineering, Komar University of Science and Technology, Sulaymaniyah, Iraq.

Acknowledgments

This experimental research project was conducted at Missouri University of Science and Technology and was funded by the Mid-America Transportation Center (MATC), and Missouri Department of Transportation (MoDOT).

Author Contributions

The authors confirm the contribution to the paper as follows: study conception and design the experiment: M. ElGawady; data collection, analysis, interpretation of results and draft manuscript preparation: B. Shrestha; critical feedback and helped shape the research: A. Gheni; editing and reviewing the manuscript: M. Abdulazeez, M. ElGawady. All authors reviewed the results and approved the final version of the manuscript.

Declaration of Conflicting Interests

The author(s) declared no potential conflicts of interest with respect to the research, authorship, and/or publication of this article.

Funding

The author(s) disclosed receipt of the following financial support for the research, authorship, and/or publication of this article: This research project was funded by the Mid-America Transportation Center (MATC), and Missouri Department of Transportation (MoDOT).

References

1. Karagah, H., C. Shi, M. Dawood, and A. Belarbi. Experimental Investigation of Short Steel Columns with Localized Corrosion. *Thin-Walled Structures,* Vol. 87, 2015, pp. 191–199.
2. Ramadan, A., and M. ElGawady. Axial Behavior of Corroded H-Piles. *IABSE 8 Congress,* New York City, NY, USA, Sept. 4th–6th, No. 9, 2019.
3. Shi, C., H. Karagah, M. Dawood, and A. Belarbi. Numerical Investigation of H-Shaped Short Steel Piles with Localized Severe Corrosion. *Engineering Structures,* Vol. 73, 2014, pp. 114–124.
4. Abdulazeez, M., B. Sherstha, E. Gomaa, A. Ramadan, and M. A. ElGawady. Bond Behavior of Steel H-Pile Bridge Columns Encased in Concrete Jackets. Presented at 98th Annual Meeting of the Transportation Research Board, Washington, D.C., 2019
5. Abdulazeez, M. M., B. Shrestha, and M. ElGawady. Retrofit of Corroded Steel H-Piles using Concrete Encased in CFRP. Presented at 10th New York City Bridge Conference, New York City, NY, USA, August 26–27, 2019.
6. Karagah, H., M. Dawood, and A. Belarbi. Experimental Study of Full-Scale Corroded Steel Bridge Piles Repaired Underwater with Grout-filled Fiber-Reinforced Polymer Jackets. *Journal of Composites for Construction,* Vol. 22, No. 3, 2018, p. 04018008.
7. Liu, X., A. Nanni, P. F. Silva, and R. A. Laboube. Rehabilitation of Steel Bridge Columns with FRP Composite Materials. *Proceedings of CCC*, 2001, pp. 10–12.
8. Wan, B., C. M. Foley, S. W. Ainge, and C. Nguyen. Procedures, Cost and Effectiveness for Deteriorated Bridge Substructure Repair. Wisconsin Highway Research Program, Wisconsin Department of Transportation, 2013.
9. Abdulazeez, M. M., K. Brown, and M. A. ElGawady. Interfacial Shear Bond Strength between Steel H-Piles and Polymer Concrete Jackets. *Transportation Research Record: Journal of the Transportation Research Board*, 2020. 2674(4): 314–324.
10. Ramadan, A., and M. ElGawady. Axial Behavior of Concrete Filled Pultruded FRP Box. *Proc., 1st Joint International Conference on Design and Construction of Smart City Components*, Cairo, Egypt, 2019.
11. de Larrard, F., and T. Sedran. Optimization of Ultra-High-Performance Concrete by the Use of a Packing Model. *Cement and Concrete Research*, Vol. 24, No. 6, 1994, pp. 997–1009.
12. Graybeal, B. Ultra-High Performance Concrete. FHWA-HRT-11-038, 2011.
13. Shafieifar, M., M. Farzad, and A. Azizinamini. Experimental and Numerical Study on Mechanical Properties of Ultra High Performance Concrete (UHPC). *Construction and Building Materials,* Vol. 156, 2017, pp. 402–411.
14. Wille, K., A. E. Naaman, and G. Parra-Montesinos. Ultra-High Performance Concrete with Compressive Strength Exceeding 150 MPa (22 ksi): A Simpler Way. *ACI Material Journal*, Vol. 108, No. 1, 2011, pp. 34–46.
15. Farhat, F., D. Nicolaides, A. Kanellopoulos, and B. L. Karihaloo. High Performance Fibre-Reinforced Cementitious Composite (CARDIFRC)–Performance and Application to Retrofitting. *Engineering Fracture Mechanics,* Vol. 74, No. 1-2, 2007, pp. 151–167.
16. Farzad, M., M. Shafieifar, and A. Azizinamini. Accelerated Retrofitting of Bridge Elements Subjected to Predominantly Axial Load using UHPC Shell. Presented at 97th Annual Meeting of Transportation Research Board, Washington, D.C., 2018.
17. Ichikawa, S., H. Matsuzaki, A. Moustafa, M. A. ElGawady, and K. Kawashima. Seismic-Resistant Bridge Columns with Ultrahigh-Performance Concrete Segments. *Journal of Bridge Engineering,* Vol. 21, No. 9, 2016, p. 04016049.
18. Perry, V. A Revolutionary New Material for New Solutions. Association of Professional Engineers and Geoscientists of the Province of Manitoba (APEGM). Ductal, 2006. http://www.apegm.mb.ca/pdf/PD_Papers/ductal.pdf.
19. Zmetra, K. M., K. F. McMullen, A. E. Zaghi, and K. Wille. Experimental Study of UHPC Repair for Corrosion-Damaged Steel Girder Ends. *Journal of Bridge Engineering,* Vol. 22, No. 8, 2017, p. 04017037.
20. Kruszewski, D., and A. E. Zaghi. Design of Various Shear Connectors for Repair of Corroded Steel Girders with

Ultra-High Performance Concrete. *Transportation Research Record: Journal of the Transportation Research Board*, 2019. 2673(2): 521–530.
21. Wang, J., J. Qi, T. Tong, Q. Xu, and H. Xiu. Static Behavior of Large Stud Shear Connectors in Steel-UHPC Composite Structures. *Engineering Structures,* Vol. 178, 2019, pp. 534–542.
22. Baena, M., L. Torres, A. Turon, and C. Miàs. Analysis of Cracking Behaviour and Tension Stiffening in FRP Reinforced Concrete Tensile Elements. *Composites Part B: Engineering,* Vol. 45, No. 1, 2013, pp. 1360–1367.
23. Matthys, S., and L. Taerwe. Concrete Slabs Reinforced with FRP Grids. I: One-Way Bending. *Journal of Composites for Construction,* Vol. 4, No. 3, 2000, pp. 145–153.
24. Sharbatdar, M. K., M. Saatcioglu, and B. Benmokrane. Seismic Flexural Behavior of Concrete Connections Reinforced with CFRP Bars and Grids. *Composite Structures,* Vol. 93, No. 10, 2011, pp. 2439–2449.
25. Michael, A., H. Hamilton III, and M. Ansley. Concrete Confinement using Carbon Fiber Reinforced Polymer Grid. *Special Publication,* Vol. 230, 2005, pp. 991–1010.
26. Meng, W., K. H. Khayat, and Y. Bao. Flexural Behaviors of Fiber-Reinforced Polymer Fabric Reinforced Ultra-High-Performance Concrete Panels. *Cement and Concrete Composites* Vol. 93, 2018, pp. 43–53.
27. Waters, T. R., V. Putz-Anderson, and A. Garg. Applications Manual for the Revised NIOSH Lifting Equation. *NIOSH Publication*, No. 94-110, Department of Health and Human Services, National Institute for Occupational Safety and Health, Cincinnati, OH, 1994.
28. Naaman, A. Textile Reinforced Cement Composites: Competitive Status and Research Directions. *International RILEM Conference on Materials Science (MatSci) I*, 2010, pp. 3–22.
29. Wang, S., A. E. Naaman, and V. C. Li. Bending Response of Hybrid Ferrocement Plates with Meshes and Fibers. *Journal of Ferrocement*, Vol. 34, No. 1, 2004, pp. 275–288.
30. ACI 549.1R. 549.1R-18: Design Guide for Ferrocement. *Technical Documents*, 2018.
32. ASTM ASTM E8/E8M-16 a: Standard Test Methods for Tension Testing of Metallic Materials. ASTM International, West Conshohocken, PA, USA, 2016.
31. A307-14e1, A. Standard Specification for Carbon Steel Bolts, Studs, and Threaded Rod 60 000 PSI Tensile Strength. ASTM International, West Conshohocken, PA, 2014.
33. ASTM F33125/F3125M-19. Standard Specification for High Strength Structural Bolts and Assemblies, Steel and Alloy Steel, Heat Treated, Inch Dimensions 120 ksi and 150 ksi Minimum Tensile Strength, and Metric Dimensions 830 MPa and 1040 MPa Minimum Tensile Strength. ASTM International, West Conshohocken, PA, 2019.
34. SP-3. Surface Preparation Specification No. 3, Power Tool Cleaning. Steel Structures Painting Council, 1995.
35. ASTM C1437. *Standard Test Method for Flow of Hydraulic Cement Mortar*. ASTM International, West Conshohocken, PA, 2007.
36. ASTM C1856/C1856M-17, A. Standard Practice for Fabricating and Testing Specimens of Ultra-High Performance Concrete. ASTM International, West Conshohocken, PA, 2017.
37. ACI318. Building Code Requirements for Structural Concrete (ACI 318-14) and Commentary on Building Code Requirements for Structural Concrete (ACI 318R-14). In ACI Committee 318, 2014.